



Title	Development of a measurement method for neutron energy spectrum in the low-energy range by combining activation foils and position-sensitive proportional counter -numerical study-
Author(s)	Fujiwara, Yu; Tamaki, Shingo; Kusaka, Sachie et al.
Citation	Applied Radiation and Isotopes. 2025, 219, p. 111719
Version Type	VoR
URL	<a href="https://hdl.handle.net/11094/100981">https://hdl.handle.net/11094/100981</a>
rights	This article is licensed under a Creative Commons Attribution-NonCommercial-NoDerivatives 4.0 International License.
Note	

*The University of Osaka Institutional Knowledge Archive : OUKA*

<https://ir.library.osaka-u.ac.jp/>

The University of Osaka



# Development of a measurement method for neutron energy spectrum in the low-energy range by combining activation foils and position-sensitive proportional counter -numerical study-

Yu Fujiwara , Shingo Tamaki, Sachie Kusaka, Fuminobu Sato, Isao Murata 

Graduate School of Engineering, Osaka University, Japan

## ARTICLE INFO

### Keywords:

Boron neutron capture therapy  
Neutron Spectroscopy  
Spectrum unfolding  
Position-sensitive proportional counter  
Foil activation

## ABSTRACT

Boron Neutron Capture Therapy (BNCT) is a promising form of radiotherapy expected to be effective in treating refractory cancers such as glioblastoma. A key factor in BNCT is the neutron energy spectrum in the epithermal range (0.5 eV–10 keV), which is challenging to evaluate due to its broad and low-energy characteristics. This study proposes a novel measurement method for the neutron energy spectrum in the epithermal range, utilizing a combination of activation foils and a position-sensitive proportional counter to capture the full energy range of neutrons in BNCT. A prototype of the spectrometer was developed, and numerical validation was performed. The results of the numerical study demonstrated that the proposed spectrometer can accurately evaluate the neutron energy spectrum across a broader energy range compared to existing methods.

## 1. Introduction

Boron Neutron Capture Therapy (BNCT) is a form of radiotherapy based on  $^{10}\text{B}(n, \alpha)^7\text{Li}$  reaction, which selectively targets tumor cells due to the limited range of the reaction's particles, approximately the size of a single cell (Locher, 1936). This specificity has made BNCT a promising treatment for refractory cancers such as glioblastoma and recurrent tumors. Recently, accelerator-based BNCT (AB-BNCT) has emerged, with operational facilities worldwide, including cyclotron-based neutron sources (C-BENS, Tanaka et al., 2011), and linac-based neutron sources (Kumada et al., 2014; Porras et al., 2020). These facilities use  $^9\text{Be}$  or  $^7\text{Li}$  targets to generate neutrons, paired with Beam Shaping Assemblies (BSAs) designed to produce epithermal neutrons ( $10^{-1}$  to  $10^4$  eV). Variations in proton energies and BSA designs result in unique neutron fields across facilities, complicating standardization. Furthermore, the neutron energy ranges recommended by IAEA (IAEA, 2023) are significantly lower than those produced by accelerators, impacting relative biological effectiveness (RBE, Blue et al., 1993). Consequently, experimental verification of neutron fields is essential for ensuring patient safety and validating facility designs (Watanabe et al., 2021).

A critical parameter of a neutron irradiation field is the neutron energy spectrum. Previous studies have explored this using several

methods such as the multi-foil activation method and Bonner Sphere Spectrometer (BSS) (Auterinen et al., 2004; Ishikawa et al., 2022; Liu et al., 2013; Shiraishi et al., 2020; Ueda et al., 2015). The multi-foil activation method employs various materials to capture neutron interactions, with each material's response unfolded into an energy spectrum. For instance, Auterinen et al. assessed neutron spectra across eight reactor-based BNCT facilities using 12 activation reactions, though the method was limited to dividing the epithermal range into 12 groups. Liu et al. improved this by addressing self-shielding effects. The BSS approach utilizes detectors with varying energy responses, each incorporating a neutron moderator and a central detector, such as a  $^3\text{He}$  proportional counter or gold activation foils. However, Ueda et al. noted that setups with only three detectors struggled to fully reproduce spectra, and the use of gold foils introduced uncertainties from self-shielding. While progress has been made to mitigate these issues (Ishikawa et al., 2022; Shiraishi et al., 2020), significant challenges remain.

To address this challenge, we developed a novel spectrometer based on a  $^3\text{He}$  position-sensitive proportional counter (PSPC) (Murata and Miyamaru, 2008). This device detects the interactions of neutrons within the  $^3\text{He}$  gas, which has a high nuclear reaction cross-section and adheres to the  $1/v$  rule, establishing a direct correlation between

This article is part of a special issue entitled: ICNCT20 published in Applied Radiation and Isotopes.

\* Corresponding author.

E-mail addresses: [fujiwara21@qr.see.eng.osaka-u.ac.jp](mailto:fujiwara21@qr.see.eng.osaka-u.ac.jp) (Y. Fujiwara), [murata@see.eng.osaka-u.ac.jp](mailto:murata@see.eng.osaka-u.ac.jp) (I. Murata).

<https://doi.org/10.1016/j.apradiso.2025.111719>

Received 15 September 2024; Received in revised form 6 January 2025; Accepted 11 February 2025

Available online 12 February 2025

0969-8043/© 2025 The Authors. Published by Elsevier Ltd. This is an open access article under the CC BY-NC-ND license (<http://creativecommons.org/licenses/by-nc-nd/4.0/>).

neutron energy and interaction depth. When neutrons enter the PSPC parallel to its detector axis, the depth signal distribution reveals the neutron energy. The energy spectrum is derived from this signal distribution through a spectrum unfolding process utilizing the spectrometer's response function. A prototype of this spectrometer, designed by our research group (Y. Osawa, 2017), was validated and demonstrated the capability to estimate energy spectra effectively in the range of 0.5 eV–1 keV. However, uncertainties persisted for neutrons exceeding 1 keV due to the spectrometer's limited energy resolution and response values. Furthermore, higher-energy neutrons (above 10 keV), although present in small quantities, are critical for radiation safety. For instance, the neutron field at C-BENS exhibits a notable peak around 40 keV (Tanaka et al., 2011). Accurate assessment of these higher-energy neutrons is essential for evaluating the safety and efficacy of BNCT irradiation fields.

To improve the spectral accuracy in the 1 keV–100 keV range, we supplemented the PSPC system with activation foils. These foils emit gamma-ray signals upon activation, corresponding to specific neutron energy ranges. By carefully selecting materials that activate within defined ranges, the gamma-ray signals provide additional neutron energy data. However, the availability of suitable materials for high-resolution spectral data is limited, and the PSPC system's sensitivity diminishes above 1 keV, leading to low energy resolution. Combining the PSPC with activation foils offers the potential to enhance the accuracy of the spectral unfolding process. Furthermore, activation foils have a minimal impact on the neutron irradiation field, ensuring the PSPC's experimental performance remains intact. Despite these advantages, no previous approach has successfully integrated response functions derived from distinct theoretical principles. This study seeks to validate this combined approach through numerical simulations.

A prototype system was modeled using MCNP-5, based on the experimental setup at the OKTAVIAN facility at Osaka University, Japan (Sumita et al., 1983). The response functions of the PSPC and activation foils were calculated in MCNP and merged as described in Section 2-1. The simulations employed JENDL 4.0 nuclear data, and distributions corresponding to experimental results were generated and unfolded into energy spectra using the method outlined in Section 2-4. The estimated spectra were then compared to a reference solution—the calculated spectrum at the exit of the epithermal column—to evaluate the accuracy and feasibility of this combined spectrometer.

## 2. Materials and methods

### 2.1. Detectors

Our spectrometer combines a PSPC with 10 activation foils. The PSPC features signal terminals on both ends, allowing it to detect signals corresponding to the position where neutrons interact with the chamber's gas, based on the principle of charge division (Fischer, 1977). In this study,  $^3\text{He}$  gas was used to fill the chamber, chosen for its high nuclear-reaction cross-section for low-energy neutrons and its one-to-one correspondence with neutron energy (Fig. 1(a)). The signal distribution from the  $^3\text{He}$  PSPC ( $Y$ ), represents the reaction depth distribution, which provides energy information about epi-thermal neutrons. This data enables derivation of the energy spectrum from the depth distribution. The PSPC used in this study measured 40 cm in length, 2.5 cm in diameter, and operated at a  $^3\text{He}$  gas pressure of 5 atm.

The spectrum unfolding method is a widely employed technique to estimate the energy spectrum from signals such as pulse height spectra detected by a detector (Knoll, 2010). In this study, the measured reaction depth distribution is converted into the neutron energy spectrum. To achieve this in numerical simulations, the PSPC is axially divided into 40 segments, each 1 cm long (Fig. 1(b)), resulting in a depth distribution represented as  $Y = [y_1, y_2, \dots, y_i \dots y_{40}]^T$ .

The reaction depth distribution is mathematically expressed as the convolution of the neutron energy spectrum and the detector response

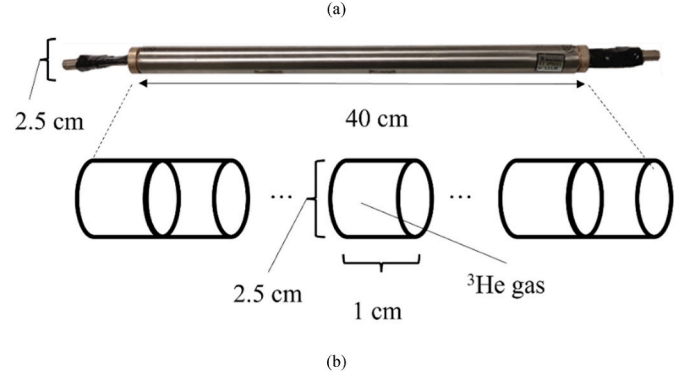
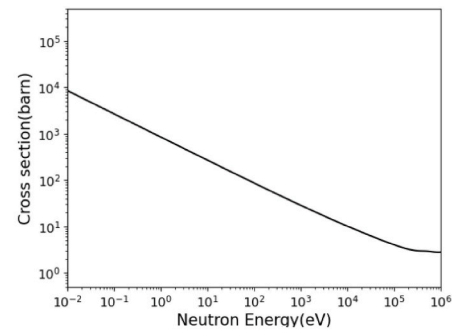


Fig. 1. Nuclear-reaction cross-sections of (a)  $^3\text{He}(n,p)^3\text{H}$  (Shibata et al., 2011) and (b) Actual PSPC and division of PSPC in the depth direction.

function. This relationship is formalized in the following equation:

$$H(r) = \int R(E, r)X(E)dE, \quad (1)$$

where  $H$  is a reaction depth distribution,  $R(E, r)$  is the response function of a spectrometer, and  $X(E)$  is the energy spectrum. The response function is the reaction depth distribution of neutron and  $^3\text{He}$ ,  $^3\text{He}(n, p)^3\text{H}$  reaction, for neutron energy. If these responses are independent, equation (1) can be rewritten as the matrix expression.

$$\begin{pmatrix} h_1 \\ \vdots \\ h_n \end{pmatrix} = \begin{pmatrix} r_{11} & \dots & r_{1m} \\ \vdots & \ddots & \vdots \\ r_{n1} & \dots & r_{nm} \end{pmatrix} \times \begin{pmatrix} x_1 \\ \vdots \\ x_m \end{pmatrix}, \quad (2)$$

where  $H$  is allotted to  $n$  bins ( $[h_1, h_2, \dots, h_i \dots h_n]^T$ ),  $X$  to  $m$  bins ( $[x_1, x_2, \dots, x_j \dots x_m]^T$ ), and then,  $R$  is defined by  $(n, m)$  matrix. To apply equation (2) to the PSPC, it was expressed as

$$\begin{pmatrix} y_1 \\ \vdots \\ y_{40} \end{pmatrix} = \begin{pmatrix} r_{11} & \dots & r_{1,53} \\ \vdots & \ddots & \vdots \\ r_{40,1} & \dots & r_{40,53} \end{pmatrix} \times \begin{pmatrix} x_1 \\ \vdots \\ x_{53} \end{pmatrix} \quad (3)$$

$X$  was divided into 53 groups ranging from 0.5 eV to 100 keV with a lethargy width of 0.1. The response function of PSPC was defined as  $R_{PSPC}$ .

As for the activation foil, it utilizes the activation reaction of some materials such as  $^{115}\text{In}(n, \gamma)^{116m}\text{In}$ ,  $^{197}\text{Au}(n, \gamma)^{198}\text{Au}$ . These materials have peaks of their activation cross-sections at their certain unique energies. The activation rate ( $A$ ) for one material is given by

$$A = N \int \sigma(E)X(E)dE, \quad (4)$$

where  $N$  is the number of target isotopes in foils,  $\sigma$  is the activation cross-section of material ( $R_{foils}$ ). If there are  $n$  pieces of information about activation rates, equation (4) can be written as following equation (5)

$$\frac{A_i}{N_i} = \sum_{j=1}^m \sigma_{ij} x_j, \quad (5)$$

where the energy spectrum was subdivided into  $m$  energy groups ( $j = 1 \sim m$ ). Additionally, equation (5) can be written as a matrix equation,

$$\begin{pmatrix} a_1 \\ \vdots \\ a_n \end{pmatrix} = \begin{pmatrix} \sigma_{11} & \cdots & \sigma_{1m} \\ \vdots & \ddots & \vdots \\ \sigma_{n1} & \cdots & \sigma_{nm} \end{pmatrix} \times \begin{pmatrix} x_1 \\ \vdots \\ x_m \end{pmatrix}, \quad (6)$$

where  $a_i = A_i/N_i$ . The energy spectrum can be described well by increasing the number of activation materials. In this research, 10 materials were selected to best reproduce the energy spectrum shown in Table 1 ( $A = [a_1, a_2, \dots, a_{10}]^T$ ) (Liu et al., 2013; Vagena et al., 2018). These materials have been widely used for neutron spectrometry. Fig. 2 shows the response ranges of selected activation foils in epi-thermal neutrons. Dy, In, Au, and W are used to evaluate neutrons in the 0.5 eV–10<sup>1</sup> eV range, Ag, Mn, and I below 1 keV neutrons, and Ni, Mo, and As are beyond the 1 keV neutrons. Notably, the width is the same as the length.

Previous studies found that PSPC was able to describe the energy spectrum from 0.5 eV to 1 keV by equation (3) (Y. Osawa, 2017). However, assessment of higher energy range is also important. Therefore, equations (3) and (6) were combined by the following equation to expand the measurable energy

$$\begin{pmatrix} y_1 \\ \vdots \\ y_{40} \\ a_1 \\ \vdots \\ a_{10} \end{pmatrix} = \begin{pmatrix} r_{11} & \cdots & r_{1,53} \\ \vdots & \ddots & \vdots \\ r_{40,1} & \cdots & r_{40,53} \\ \sigma_{11} & \cdots & \sigma_{1,53} \\ \vdots & \ddots & \vdots \\ \sigma_{10,1} & \cdots & \sigma_{10,53} \end{pmatrix} \times \begin{pmatrix} x_1 \\ \vdots \\ x_{53} \end{pmatrix} \quad (7)$$

Replacing the left-hand side by  $Z$  and the merged response function by  $R^*$ , equation (7) becomes

$$\begin{pmatrix} z_1 \\ \vdots \\ z_{50} \end{pmatrix} = \begin{pmatrix} r_{11}^* & \cdots & r_{1,53}^* \\ \vdots & \ddots & \vdots \\ r_{50,1}^* & \cdots & r_{50,53}^* \end{pmatrix} \times \begin{pmatrix} x_1 \\ \vdots \\ x_{53} \end{pmatrix} \quad (8)$$

Activation foil data, denoted as "A," is crucial for enhancing the accuracy of spectrum unfolding by providing additional energy-specific information. The inherent limitation of the PSPC's length restricts the axial division to a maximum of 40 groups, resulting in challenges when reproducing the neutron energy spectrum up to 10 keV (Fujiwara et al., 2025; Murata and Miyamaru, 2008; Osawa et al., 2017). Therefore, additional information from activation foils, especially at the higher energy range, helps to improve this accuracy.

### 2.2. Application of Bayesian estimation

In this section, the solution method for Equation (8) is described. Because experimental results, such as pulse height spectra, contain statistical errors, the signal distribution cannot be directly converted into the energy spectrum. Various approaches, such as the Least Squares and Maximum Likelihood Methods, have been explored to address this issue (Cvachovec and Cvachovec, 2008). In this study, Bayesian estimation was applied to unfold the energy spectrum (Iwasaki et al., 1997). This approach was deduced purely only from the Bayes' Theorem

$$P(A|B) = \frac{P(B|A) \times P(A)}{P(B)} \quad (9)$$

where  $P$  refers to probability, and the meaning of each probability is shown below.

- $P(A)$ : Initial neutron energy spectrum as the prior probability
- $P(B)$ : Probability of a signal detected by the spectrometer which is the normalization in Bayes' theorem.
- $P(A|B)$ : Posterior probability of the energy spectrum when a prior probability was given.
- $P(B|A)$ : Likelihood as the response function, which is the signal distribution for a certain neutron energy.

Therefore, given the response function and the experimental signal distribution, the energy spectrum can theoretically be determined regardless of the initial value. This is one of the main advantages of this approach, whereas the least squares approach faces this limitation. Nauchi applied Bayesian estimation to spectrum unfolding using Equation (9) (Nauchi and Iwasaki, 2014);

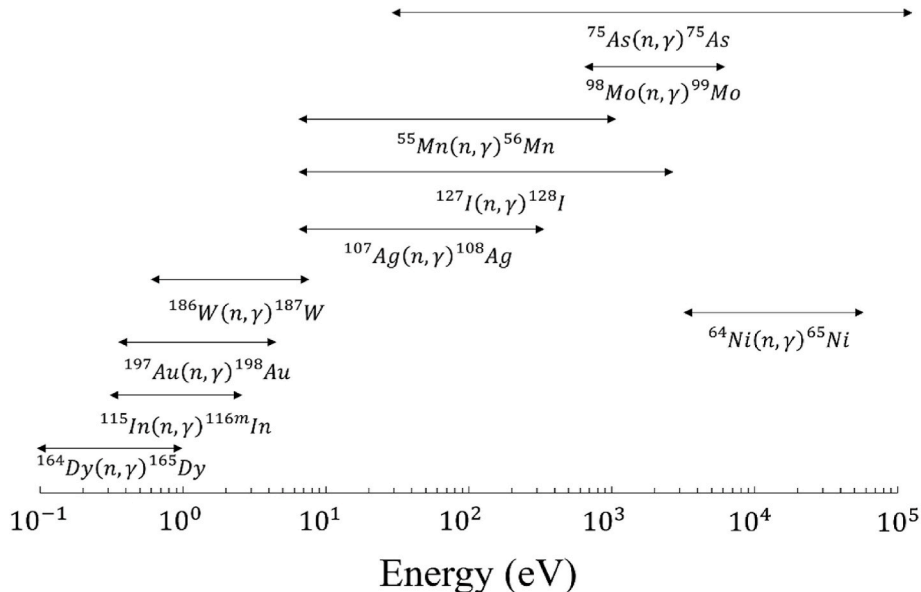


Fig. 2. Response of the selected activation foils set-up in epi-thermal range.

$$est_j^{(k+1)} = \sum_i z_i \frac{r_{ij}^* \times est_j^{(k)}}{\sum_j est_j^{(k)} \times r_{ij}^*} \quad (10)$$

Where,  $est_j^{(k)}$  is the  $j$  th value of the energy spectrum with  $k$  times iteration of this algorithm ( $0 \leq j \leq 53$ ), and  $i$  takes values from 1 to 50.  $r_{ij}^*$  means the  $(i, j)$  values of  $r^*$ . Note that we introduced the uninformed distribution, where all values are  $1/n$ , as the initial spectrum ( $est^{(1)} = \{1\}$ ).

2.3. 2-3. Experimental set-up

Fig. 2 (a) illustrates the prototype design of the spectrometer, which includes an Epi-thermal column, and a spectrometer based on the OKTAVIAN accelerator (Sumita et al., 1983). This system uses a DT neutron source that generates 14 MeV neutrons. A 300 keV deuterium ion beam is produced by a Cockcroft-Walton type accelerator with a duoplasmatron ion source. The continuous neutron source has a maximum intensity of approximately  $3 \times 10^{12}$  DT neutrons per second (Tamaki et al., 2022). Osawa et al. designed the epi-thermal column using materials like iron, carbon, lead, and aluminum fluoride to provide adequate neutron flux for various experiments (Fig. 2 (b)) (Osawa et al., 2017). In this study, the energy spectrum calculated at the exit of the epi-thermal column using the F2 tally in MCNP serves as the reference (reference flux,  $ref$ , shown in Fig. 3). The PSPC was placed 70 cm behind the epi-thermal column inside a collimator hole in the concrete wall of the experimental room to prevent side-surface neutrons from distorting the signal (Fujiwara et al., 2024). Activation foils were positioned around the collimator hole (Fig. 2 (c)). The thickness and lengths were defined in (Fig. 2 (c)), with their thickness and length specified in Table 1.

2.4. Numerical experiment

To confirm the accuracy of our approach theoretically, numerical experiments were conducted by several candidates of  $Z$  (i) in equation

**Table 1**  
Material selection for activation foils.

Materials	Length ( $L$ , cm)	Thicknesses ( $T$ , cm)	Reaction
In	1	0.5	$^{115}\text{In} (n, \gamma)^{116m}\text{In}$
Au	1	0.5	$^{197}\text{Au} (n, \gamma)^{198}\text{Au}$
I	3	1	$^{127}\text{I} (n, \gamma)^{128}\text{I}$
As	3	1	$^{75}\text{As} (n, \gamma)^{76}\text{As}$
Ag	3	1	$^{107}\text{Ag} (n, \gamma)^{108}\text{Ag}$
W	1	0.5	$^{186}\text{W} (n, \gamma)^{187}\text{W}$
Ni	3	1	$^{64}\text{Ni} (n, \gamma)^{65}\text{Ni}$
Mn	3	1	$^{55}\text{Mn} (n, \gamma)^{56}\text{Mn}$
Mo	3	1	$^{98}\text{Mo} (n, \gamma)^{99}\text{Mo}$
Dy	1	0.5	$^{164}\text{Dy} (n, \gamma)^{165}\text{Dy}$

(8) listed below. First of all,  $ref$  was calculated and folding result with (8),  $est$  values were estimated by equation (10) in each case;

- Z (1): The matrix of  $R^*$  and  $ref$ ,  $R^* ref$ ,
- Z (2):  $R^* ref + \varepsilon_1$  (=1% normal distribution),
- Z (3):  $R^* ref + \varepsilon_2$  (=3% normal distribution),
- Z (4):  $R^* ref + \varepsilon_3$  (=5% normal distribution),
- Z (4):  $R^* ref + \varepsilon_4$  (=10% normal distribution),

where  $\varepsilon$  represents the counting error. In the real experiment, the count itself reflects the magnitude of the statistical error. Numerical experiments help determine the permissible tolerance for statistical errors. Excessively large counting errors can cause divergence in the estimated results. Thus, the tolerance range for these errors was investigated by adding a hypothetical error value. The Monte Carlo simulation code, MCNP 5, evaluated the response functions of the two detectors,  $R_{PSPC}$  and  $R_{foils}$ , using the nuclear data library JENDL-4.0 (Shibata et al., 2011). The response defined in equation (7) was determined using the  $^3\text{He} (n, p)$  reaction rate ( $r_{k,m}$ ) for the spectrometer and the response of each foil through the  $(n, \gamma)$  reaction, with the corresponding cross-section ( $\sigma_{q,m}$ ) for each energy, calculated in the following equations.

$$r_{k,m} = M_k(E = E_m) \times \pi r^2 \times d \quad (11)$$

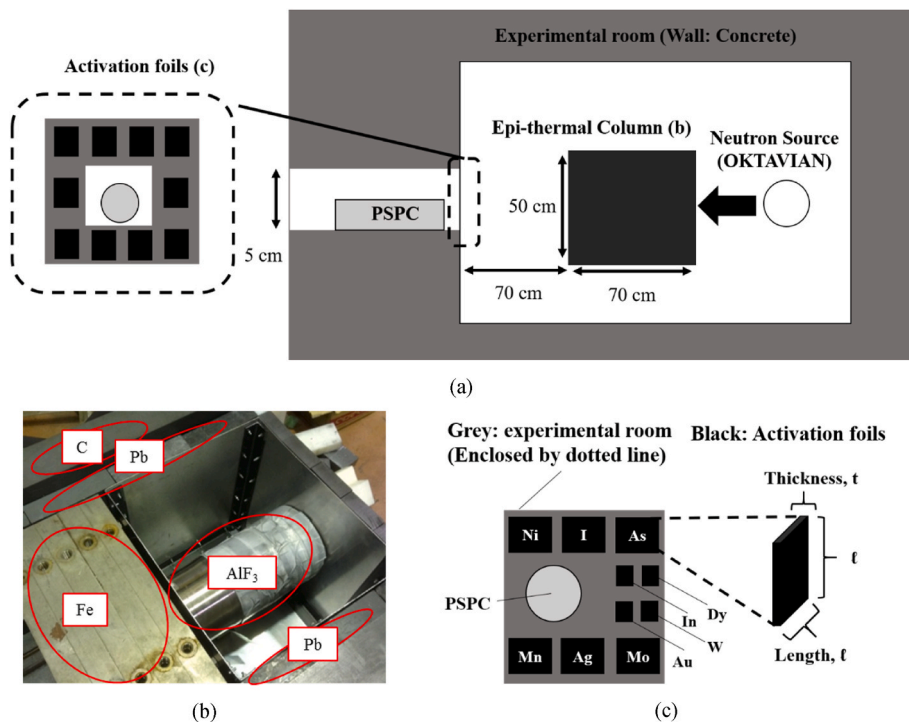


**Fig. 3.** Experimental System. (a) Overall Geometry of the Experimental System, (b) Epi-thermal Column, (c) Deployment of the activation foils.

$$\sigma_{q,m} = O_q(E = E_m) \times L_q^2 \times T_q \quad (12)$$

Where  $M_k$  is the reaction rate of the (n, p) reaction at the k th interval of the PSPC, calculated using the F4 tally in MCNP, r is the radius of the PSPC, and d is the division interval of the PSPC (cm, with d = 1. For the activation foils, q'' represents the material number, O is the (n,  $\gamma$ ) reaction rate calculated using the F4 tally in MCNP, L is the length, T is the thickness of the foils. The energy spectrum estimated using equation (10) was compared to the *ref*. Then, their response functions were merged and applied to the unfolding process.

### 3. Results

Fig. 4 shows the response functions of each detector ( $R_{PSPC}$ , (a) and  $R_{foils}$ , (b)) calculated using equations (11) and (12). The shape of  $R_{PSPC}$  indicates that the response decreases with the detector's depth, while  $R_{foils}$  exhibits a peak at specific energies corresponding to each material's activation cross-sections. Using the combined response function  $R^*$ , shown in Fig. 5 (c), the energy spectrum was deduced numerically using equation (10), as shown in Fig. 6. The "Simulation" label refers to the reference (ref), and the colored spectra represent the estimation values (est) from Z (1)–(4). The estimated spectrum generally agrees with the reference solution and reproduces the characteristic shape in cases (1)–(3). In case (4), larger discrepancies were observed between *ref* and *est* compared to other cases. However, *est* values were significantly higher than *ref* values for higher-energy neutrons. Additionally, common peak-like features appear around 10 eV and 20 eV, which is discussed in the Discussion section. To quantify the unfolding performance of this approach, Spectral Angle Mapper (SAM) and Mean Absolute Percentage Error (MAPE) were introduced. The SAM criterion, which depends on the spectral angle between est and ref, it was used to assess shape similarity (Zhu et al., 2019). The equation for SAM is given in (13), where spectra that are similar will yield a value close to 0.

$$SAM(ref, est) = \cos^{-1} \left( \frac{ref \cdot est}{\|ref\| \cdot \|est\|} \right) = \cos^{-1} \left( \frac{\sum_j ref_j \cdot est_j}{\sqrt{\sum_j ref_j^2} \sqrt{\sum_j est_j^2}} \right) \quad (13)$$

On the other hand, MAPE focuses on the numerical error as shown in equation (14).

$$MAPE = \frac{100}{53} \sum_j \left| \frac{est_j - ref_j}{ref_j} \right| \quad (14)$$

MAPE is insufficient for assessing shape similarity, even when the error is minimal. Combining SAM and MAPE enables quantitative evaluation of estimation accuracy. In this study, predictions were deemed good when SAM and MAPE were under 20%. Due to discrepancies in the higher-energy range, statistical analyses focused on neutrons up to 10 keV. Table 2 presents the statistical analysis results, showing that both SAM and MAPE increased with larger errors. Nevertheless, the model demonstrated robustness within a 3% uncertainty, meeting the numerical targets. Fig. 7 compares the results of this approach with a previous method (Murata and Miyamaru, 2008). This study evaluated the PSPC response theoretically by (15) given in

$$R(y, E) dy = \Sigma(E) \cdot \exp(-\Sigma(E)y) dy, \quad (15)$$

Where  $\Sigma(E)$  is the macroscopic cross-section which is defined by microscopic nuclear-reaction cross-section and atomic number density,

$$\Sigma(E) = n \cdot \sigma(E) \quad (16)$$

The estimation was performed under the same conditions as Z (1), using experimental data derived from the convolution of the spectrum and response function without considering errors. The current approach significantly improved estimation accuracy, particularly in higher-energy regions.

### 4. Discussion

Numerical experiments indicated that the merged and calculated response function could unfold the energy spectrum from the input values, matching the experimental results. Fig. 6 shows that the accuracy of the estimated spectra agrees well with the *ref* except for case (4). These results reveal experimental conditions. The errors are added to the matrix by counting errors, which generally adhere to Poisson distribution. From the results in Table 2, the valuable spectrum can be estimated within 3% of counting errors, requiring over 1200 counts for each activation foil. This allows the experimental time to be determined.

However, the sharp decline in the higher-energy range was not represented excellently. To derive the valuable spectrum from the true experimental data, several considerations are needed to improve estimation accuracy:

- I. **The calculated error for the response function.** The response function in Fig. 4 (a) contained a calculation error in the MC simulation. Even small errors can significantly impact the accuracy of iterations of equation (10).
- II. **Selection of more suitable materials.** As shown in Fig. 7, improvements in the higher-energy regions were due to activation foils, which provided more information about epi-thermal neutrons. This combination approach effectively evaluates the energy spectrum. However, peaks in the estimated spectrum at 1 eV, 10 eV, and 20 eV are thought to result from the high responses of In, Au, W, and I at their respective energies, as shown in Fig. 5(b). To mitigate this impact, using cadmium to cut off thermal neutrons or optimizing foil arrangements may be effective.

Notably, the estimated spectra showed good agreement with the reference spectrum, despite equations (3) and (6) being based on different physical laws, the former is based on protons by  $^3\text{He}$  (n, p)  $^3\text{H}$  reaction in PSPC, while equation (6) is based on activation reactions in various materials. Generally, signals governed by different physical laws are not used for spectrum unfolding due to the drastic changes in the response function's shape (Fig. 5). Nonetheless, the estimated spectra reproduced the reference spectrum well, likely because the number of Z increased, and the absolute values in both detectors did not change

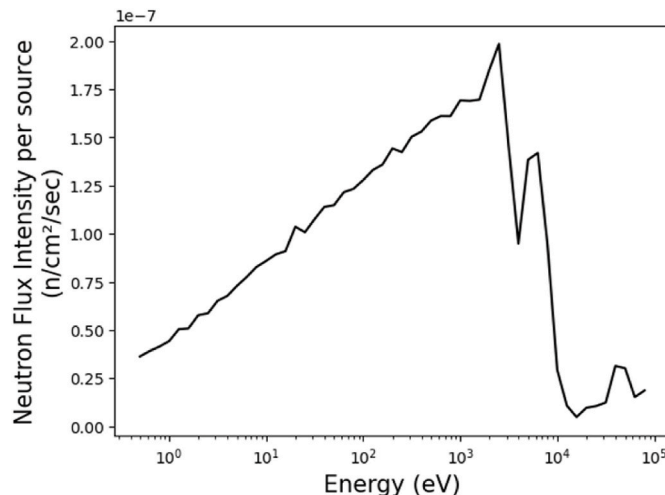


Fig. 4. Reference flux (*ref*) calculated at the exit of the epi-thermal column.

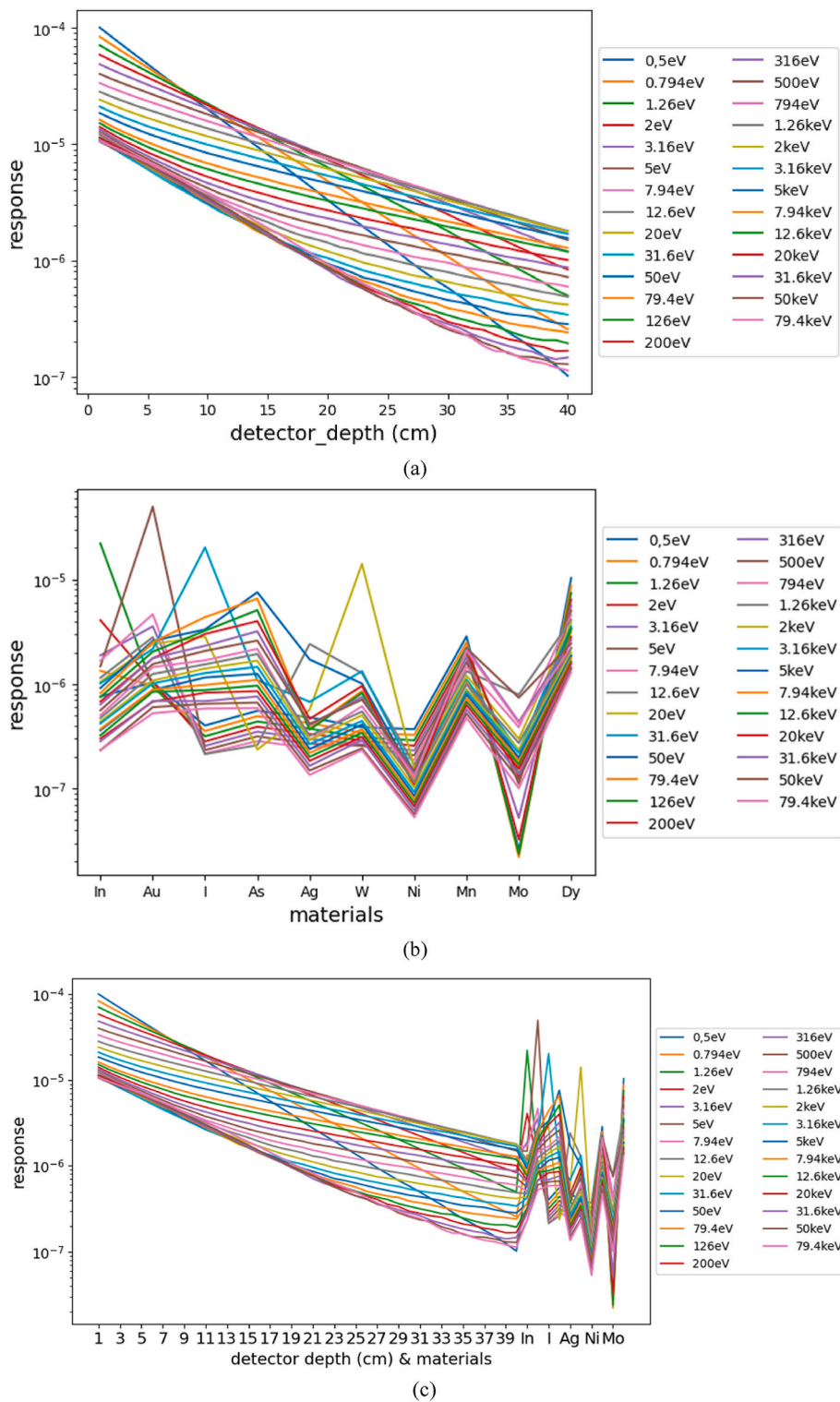


Fig. 5. (a, b) Calculated Response Function  $R$  and  $\sigma$  (a: PSPC, b: Activation foils) (c) Merged and normalized Response Function  $R^*$ .

significantly. This result demonstrates that the experimental data can be converted simultaneously into the energy spectrum, even if it consists of signals produced by different physical phenomena.

Conventionally, the multi-foil method using activation foils requires an initial guess (Sakurai and Kobayashi, 2004), which introduces a dependency on the initial spectrum values. Furthermore, there are insufficient materials to describe the entire epi-thermal neutron energy

range, making the accuracy of this approach contentious. However, our presented method overcomes this issue. The estimated energy spectrum was reproduced using an uninformed prior distribution, with PSPC and activation foils complementing each other's information.

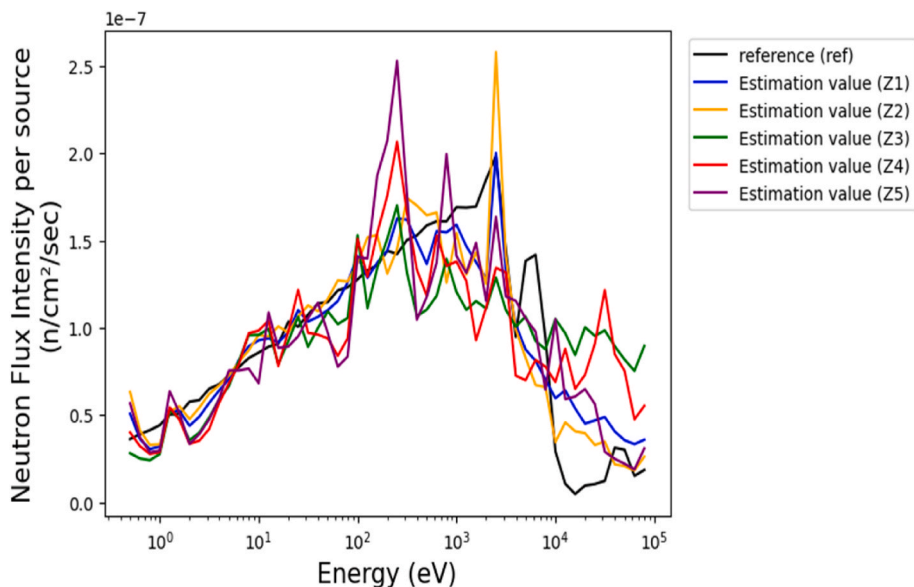


Fig. 6. Comparison of ref vs est.

Table 2

Results of the statistical tests (up to 10 keV).

	SAM (degree)	MAPE (%)
Z (1)	8.39	11.27
Z (2)	11.32	13.38
Z (3)	11.69	19.57
Z (4)	14.68	21.21
Z (5)	16.03	22.12

5. Conclusion

This study aimed to evaluate the effectiveness of a novel approach for estimating the neutron energy spectrum in the epi-thermal range, a critical parameter for assessing human exposure during BNCT treatment. The proposed method combines a position-sensitive proportional counter with activation foils. While each technique has limitations in its

measurable range, its integration allows coverage over a broader spectrum. By modeling the response of each detector and simulating signal distribution by the MC simulation, the energy spectrum was estimated and compared to a reference spectrum through the spectrum unfolding technique. Bayesian estimation was employed to solve the inverse problem, enabling spectrum derivation from any initial value. To account for experimental conditions, several normal distributions with errors were added to the counting values. The results demonstrated good agreement between the estimated and reference values up to 10 keV. This indicates that incorporating activation foils improves spectrum unfolding performance, leading to a more accurate reproduction of the energy spectrum. Notably, the findings suggest that spectrum unfolding may be applicable when merging different physical measurements. However, the estimated values did not replicate the sharp decrease in the spectrum above 10 keV. Analysis using SAM and MAPE confirmed that this approach effectively measures the neutron energy spectrum in the epi-thermal range with high robustness. Furthermore, optimizing

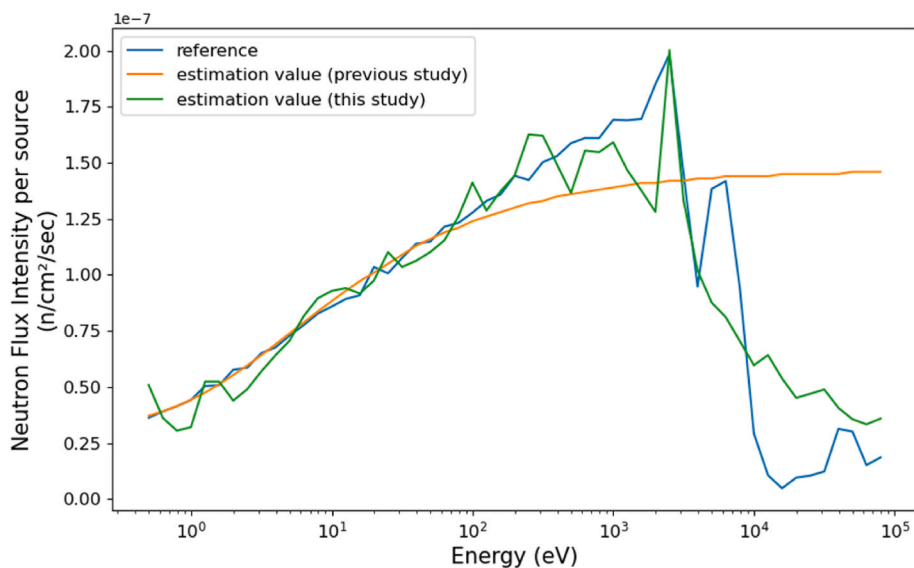


Fig. 7. Reference spectrum (blue line), estimated values from the PSPC alone (previous study, orange line) and the combination of PSPC with the Multi-Foil activation method (Z (1) value of this study, green line). Compared to the previous approach, the proposed method accurately reproduces the sharp reduction in the spectrum at higher-energy neutrons.

the arrangement and dimensions of activation foils could enhance the performance of this spectrometer.

### CRedit authorship contribution statement

**Yu Fujiwara:** Writing – original draft, Visualization, Validation, Methodology, Investigation, Funding acquisition, Formal analysis, Data curation, Conceptualization. **Shingo Tamaki:** Software. **Sachie Kusaka:** Resources. **Fuminobu Sato:** Project administration. **Isao Murata:** Writing – review & editing, Supervision.

### Funding sources

JSPS KAKENHI Grant-in-Aid supported this work for Fellows Number 24KJ1616.

### Declaration of competing interest

The authors declare the following financial interests/personal relationships which may be considered as potential competing interests: Yu Fujiwara reports financial support was provided by Japan Society for the Promotion of Science. If there are other authors, they declare that they have no known competing financial interests or personal relationships that could have appeared to influence the work reported in this paper.

### Data availability

The data that has been used is confidential.

### References

- Auterinen, I., Serén, T., Anttila, K., Kosunen, A., Savolainen, S., 2004. Measurement of free beam neutron spectra at eight BNCT facilities worldwide. *Appl. Radiat. Isot.* 61 (5). <https://doi.org/10.1016/j.apradiso.2004.05.035>.
- Blue, T.E., Gupta, N., Woollard, J.E., 1993. A calculation of the energy dependence of the RBE of neutrons. *Phys. Med. Biol.* 38 (12). <https://doi.org/10.1088/0031-9155/38/12/002>.
- Cvachovec, J., Cvachovec, F., 2008. Maximum likelihood estimation of a neutron spectrum and associated uncertainties. *Advances in Military Technology* 3 (2).
- Fischer, B.E., 1977. A digital processor for position sensitive detectors. *Nucl. Instrum. Methods* 141 (1). [https://doi.org/10.1016/0029-554X\(77\)90763-7](https://doi.org/10.1016/0029-554X(77)90763-7).
- Fujiwara, Y., Tamaki, S., Kusaka, S., Sato, F., Murata, I., 2024. Validation of low-energy neutron spectrometer using a position-sensitive proportional counter -design and fabrication of beam neutron source-. *Radiation Detectors And Their Uses* 158–168. IAEA, 2023. *Advances in Boron Neutron Capture Therapy. INTERNATIONAL ATOMIC ENERGY AGENCY.*
- Ishikawa, A., Watanabe, K., Yamazaki, A., Yoshihashi, S., Imai, S., Masuda, A., Matsumoto, T., Tanaka, H., Sakurai, Y., Nogami, M., Hitomi, K., Uritani, A., Harano, H., 2022. Evaluation of the thermal neutron sensitivity, output linearity, and gamma-ray response of optical fiber-based neutron detectors using Li-glass scintillator. *Nucl. Instrum. Methods Phys. Res. Sect. A Accel. Spectrom. Detect. Assoc. Equip.* 1025. <https://doi.org/10.1016/j.nima.2021.166074>.
- Iwasaki, S., Odanaka, S., Mitsui, T., Kitamura, M., 1997. A proposed algorithm for adaptive computer tomography. *Appl. Radiat. Isot.* 48 (10–12). [https://doi.org/10.1016/S0969-8043\(97\)00140-1](https://doi.org/10.1016/S0969-8043(97)00140-1).
- Knoll, Glenn F., 2010. *Radiation Detection and Measurement, 4th ed.*
- Kumada, H., Matsumura, A., Sakurai, H., Sakae, T., Yoshioka, M., Kobayashi, H., Matsumoto, H., Kiyanagi, Y., Shibata, T., Nakashima, H., 2014. Project for the development of the linac based NCT facility in University of Tsukuba. *Appl. Radiat. Isot.* 88. <https://doi.org/10.1016/j.apradiso.2014.02.018>.
- Liu, Y.H., Chen, W.L., Jiang, S.H., 2013. Improvement of activation-detector-based spectrum unfolding technique for BNCT. *IEEE Trans. Nucl. Sci.* 60 (2). <https://doi.org/10.1109/TNS.2012.2235463>.
- Locher, G.L., 1936. Biological effects and therapeutic possibilities of neutrons. *Am. J. Roentgenol. Radium Ther.* 36.
- Murata, I., Miyamaru, H., 2008. Low-energy neutron spectrometer using position sensitive proportional counter-Feasibility study based on numerical analysis. *Nucl. Instrum. Methods Phys. Res. Sect. A Accel. Spectrom. Detect. Assoc. Equip.* 589 (3). <https://doi.org/10.1016/j.nima.2008.02.071>.
- Nauchi, Y., Iwasaki, S., 2014. Convergence of unfolded spectrum with response function for single radiation based on Bayes' theorem. *Nucl. Instrum. Methods Phys. Res. Sect. A Accel. Spectrom. Detect. Assoc. Equip.* 735. <https://doi.org/10.1016/j.nima.2013.09.064>.
- Fujiwara, Y., Tamaki, S., Sato, F., Murata, I., 2025. Development of a new low-energy neutron spectrometer using a position-sensitive proportional counter: examination of the response function considering the spectrometer shield. *J. Radiat. Prot. Res.* <https://doi.org/10.14407/jrpr.2023.00325>.
- Y. Osawa. (2017). Master Dissertation. Osaka University.
- Osawa, Y., Imoto, S., Kusaka, S., Sato, F., Tanoshita, M., Murata, I., 2017. Development of an epi-thermal neutron field for fundamental researches for BNCT with a DT neutron source. *EPJ Web Conf.* 153. <https://doi.org/10.1051/epjconf/201715304008>.
- Porrás, I., Praena, J., Arias de Saavedra, F., Pedrosa-Rivera, M., Torres-Sánchez, P., Sabariego, M.P., Expósito-Hernández, J., Llamas-Elvira, J.M., Ramírez-Navarro, A., Rodríguez-Fernández, A., Osorio-Ceballos, J.M., Ruiz-Ruiz, C., Ruiz-Magaña, M.J., 2020. BNCT research activities at the Granada group and the project NeMeSis: neutrons for medicine and sciences, towards an accelerator-based facility for new BNCT therapies, medical isotope production and other scientific neutron applications. *Appl. Radiat. Isot.* 165. <https://doi.org/10.1016/j.apradiso.2020.109247>.
- Sakurai, Y., Kobayashi, T., 2004. Spectrum evaluation at the filter-modified neutron irradiation field for neutron capture therapy in Kyoto University Research Reactor. *Nucl. Instrum. Methods Phys. Res. Sect. A Accel. Spectrom. Detect. Assoc. Equip.* 531 (3). <https://doi.org/10.1016/j.nima.2004.05.084>.
- Shibata, K., Iwamoto, O., Nakagawa, T., Iwamoto, N., Ichihara, A., Kunieda, S., Chiba, S., Furutaka, K., Otuka, N., Ohsawa, T., Murata, T., Matsunobu, H., Zukeran, A., Kamada, S., Katakura, J.I., 2011. JENDL-4.0: a new library for nuclear science and engineering. *J. Nucl. Sci. Technol.* 48 (1). <https://doi.org/10.1080/18811248.2011.9711675>.
- Shiraishi, S., Takata, T., Tanaka, H., Sakurai, Y., 2020. A study on remotely-changeable moderators in Bonner sphere spectrometer for irradiation-field characterization in boron neutron capture therapy. *Appl. Radiat. Isot.* 163. <https://doi.org/10.1016/j.apradiso.2020.109213>.
- Sumita, K., Takahashi, A., Iida, T., Yamamoto, J., Imoto, S., Matsuda, K., 1983. OSAKA UNIVERSITY 14meV INTENSE NEUTRON SOURCE and its UTILIZATIONS for FUSION STUDIES (OKTAVIAN PROGRAM). <https://doi.org/10.1016/b978-1-4832-8374-6.50096-4>. Commission of the European Communities, (Report) EUR, 1.
- Tamaki, S., Panuntun, F., Uedoi, K., Haidong, W., Kusaka, S., Manabe, Y., Akiyama, Y., Tanaka, T., Sato, F., Murata, I., 2022. Radioactivation analysis of concrete wall in OKTAVIAN facility. *Plasma Fusion Res.* 17. <https://doi.org/10.1585/PFR.17.1405001>.
- Tanaka, H., Sakurai, Y., Suzuki, M., Masunaga, S., Mitsumoto, T., Fujita, K., Kashino, G., Kinashi, Y., Liu, Y., Takada, M., Ono, K., Maruhashi, A., 2011. Experimental verification of beam characteristics for cyclotron-based epithermal neutron source (C-BENS). *Appl. Radiat. Isot.* 69 (12). <https://doi.org/10.1016/j.apradiso.2011.03.020>.
- Ueda, H., Tanaka, H., Sakurai, Y., 2015. Reprint of the improvement of the energy resolution in epi-thermal neutron region of Bonner sphere using boric acid water solution moderator. *Appl. Radiat. Isot.* 106. <https://doi.org/10.1016/j.apradiso.2015.10.010>.
- Vagena, E., Theodorou, K., Stoulos, S., 2018. Thick-foils activation technique for neutron spectrum unfolding with the MINUIT routine—Comparison with GEANT4 simulations. *Nucl. Instrum. Methods Phys. Res. Sect. A Accel. Spectrom. Detect. Assoc. Equip.* 887. <https://doi.org/10.1016/j.nima.2018.01.025>.
- Watanabe, K., Yoshihashi, S., Ishikawa, A., Honda, S., Yamazaki, A., Tsurita, Y., Uritani, A., Tsuchida, K., Kiyanagi, Y., 2021. First experimental verification of the neutron field of Nagoya University Accelerator-driven neutron source for boron neutron capture therapy. *Appl. Radiat. Isot.* 168. <https://doi.org/10.1016/j.apradiso.2020.109553>.
- Zhu, H., Altmann, Y., di Fulvio, A., McLaughlin, S., Pozzi, S., Hero, A., 2019. A hierarchical Bayesian approach to neutron spectrum unfolding with organic scintillators. *IEEE Trans. Nucl. Sci.* 66 (10). <https://doi.org/10.1109/TNS.2019.2941317>.